https://doi.org/10.5194/egusphere-2026-341
Preprint. Discussion started: 17 March 2026

Quantifying the impact of vehicle fleet electrification on local aerosol concentrations in Helsinki using high-resolution Large Eddy Simulation

Nahid Atashi[1,8], Xiaoyu Li[1], Sasu Karttunen[2,3], Riku Viri[4], Roy Harrison[5], Jani Strömberg[1], Aino Kaltianen[6], Matti Leinonen[7], Laura Ruotsalainen[5,8], and Leena Järvi[1,8]

[1]Institute for Atmospheric and Earth System Research (INAR/Physics), Faculty of Science, University of Helsinki, Helsinki, 00014, Finland.
[2]School of Engineering and Computer Science, Bern University of Applied Sciences, Biel/Bienne, Switzerland.
[3]Department of Geoscience and Remote Sensing, Delft University of Technology, Delft, The Netherlands.
[4]Faculty of Built Environment, Tampere University, Tampere, Finland.
[5]Division of Environmental Health Risk Management, School of Geography, Earth Environmental Sciences, University of Birmingham, Edgbaston, Birmingham, United Kingdom.
[6]Department of Meteorology, Stockholm University, Stockholm, Sweden.
[7]Department of Computer Science, Faculty of Science, University of Helsinki, Helsinki, 00014, Finland.
[8]Helsinki Institute of Sustainability Science (HELSUS), University of Helsinki, Helsinki, Finland.

Correspondence: Nahid Atashi (nahid.atashi@helsinki.fi)

Abstract. Urban air quality strategies increasingly rely on transitioning to battery electric vehicles (BEVs), yet their impact on non-exhaust aerosol emissions remains uncertain. This study uses high-resolution Large Eddy Simulation (LES) to investigate aerosol concentrations in a planned Helsinki neighborhood where a highway corridor is being converted into a residential boulevard. We consider three scenarios with varying BEVs shares: a baseline year 2022 (10% of BEVs), and projected years 2035 (60%) and 2040 (100%).

The findings reveal a "dual impact" of vehicle electrification. Increased BEV shares significantly reduce particle number concentrations $PN_{2.5}$, with a projected 60% decrease by 2040 compared to the baseline. Conversely, fine particle mass $PM_{2.5}$ is projected to increase by approximately 15% by 2040. This divergence occurs because while BEVs eliminate tailpipe exhaust, their greater weight increases unregulated non-exhaust emissions (NEE) from tire and brake wear. Results show high spatial variation, with pollutants concentrated along boulevard roads and limited penetration into residential blocks. This study underscores the challenges of BEV adoption in realistic urban environments and provides vital insights for sustainable urban planning and pollution mitigation strategies.

1 Introduction

Air pollution is one of the major environmental risks to human health and is perceived as the second largest environmental concern after climate change. Exposure to air pollution has been estimated to cause approximately 0.8 million premature deaths annually in Europe (Lelieveld et al., 2019). In Finland, 1600-2000 premature deaths are attributable to air pollution per year

https://doi.org/10.5194/egusphere-2026-341
Preprint. Discussion started: 17 March 2026

(Lehtomäki et al., 2018). According to the 2024 State of Global Air report (SoGA, 2024), air pollution was responsible for 8.1 million deaths worldwide in 2021, making it the second leading risk factor for mortality.

Since the European Union (EU) began addressing air quality issues in the late 1970s, there have been notable reductions in emissions of key air pollutants and their concentrations in ambient air. Despite these advances, exceedance of air quality standards remains common, and the majority of the urban population of the EU region is still exposed to harmful levels of air pollution. Specifically, 96% of urban residents are exposed to $PM_{2.5}$ concentrations above WHO (World Health Organization) recommended levels, 95% to ozone, and 89% to NO_2 (Vivienne, 2023). Road traffic has been identified as the dominant source of air pollutants in cities (Fenger, 2009), and consequently the highest levels of pollution are commonly seen at the pedestrian level in poorly ventilated streets with heavy traffic (Vardoulakis et al., 2003). Although the primary sources of pollutants and their dispersion patterns in urban areas have been widely identified, accurately predicting air quality within urban neighborhoods remains a challenge because traditionally used air quality models are insufficient to solve complex flow and pollutant distributions that occur in complex urban landscapes. This limitation hinders our ability to fully understand the behavior of pollutants and make reliable air quality predictions at the neighborhood and street levels (Chen et al., 2017; Tominaga and Stathopoulos, 2016). The most novel tool to resolve the three-dimensional pollutant distributions within real urban neighborhoods is the Large Eddy Simulation (LES) (Salim et al., 2011). In LES, the prognostic equations for flow, temperature, and other scalars are numerically solved for large-scale turbulent motion, whereas the subgrid-scale processes are parameterized. LES has been shown to provide an improved representation of pollutant dispersion in complex urban settings compared to Reynolds-averaged Navier-Stokes equations with parameterized turbulence, as these models cannot capture the inherently unsteady plume dynamics driven by urban geometry (Harms et al., 2011; Gousseau et al., 2011; García-Sánchez et al., 2018). Recent advances in computational capacity have made LES applicable in complex environments, enabling highly resolved air pollution and turbulence simulations up to 1 m in areas where traditional air quality models often fail (Zhang et al., 2021; Kurppa et al., 2018a; Tolias et al., 2018).

Several actors from cities to the EU have established clear goals to reduce air pollution and greenhouse gas emissions. For example, the City of Helsinki has set a target to achieve carbon neutrality by 2035 (city of Helsinki, 2018). The use of new driving power technologies in both passenger and public transport is one of the key components to achieve these goals. The European Environment Agency (EEA, 2023) reported considerable progress of 22% of new car registrations being electric vehicles in EU countries in 2022, totaling about two million electric car registrations in one year. This was a considerable increase compared to the previous year 2021 with about 1,74 million electric cars registered. According to the regional vehicle fleet model (SALAMA) for Finland, the number of electric passenger cars is expected to reach 320,000, both Battery Electric Vehicles (BEV) and Plug-in Hybrid Electric Vehicles (PHEV), in 2035 and 830,000 in 2040 (Viri et al., 2021). The increasing number of BEVs will certainly decrease tailpipe exhaust emissions, but their overall impact on local aerosol particle concentrations remains unclear. BEVs might significantly contribute to non-exhaust emissions (NEE) of brakes and tires, road surface abrasion and road dust resuspension (Piscitello et al., 2021; Fussell et al., 2022). NEE is expected to be higher from BEVs than from traditional internal combustion engine vehicles (ICEVs), because BEVs are generally heavier, leading to increased tire, brake, and road surface wear emissions, and are often equipped with all- or four-wheel drive systems, compared

https://doi.org/10.5194/egusphere-2026-341
Preprint. Discussion started: 17 March 2026

to front-wheel or rear-wheel drive systems typically found in ICEVs, which can further contribute to higher wear emissions (Hooftman et al., 2018; Liu et al., 2022). According to a review by Harrison et al. (2021), the contribution of NEE to total road transport emissions of $PM_{2.5}$ is projected to increase in Europe from 50% in 2018 to 71% in 2035. NEE is expected to become the main source of traffic-related particulate matter by 2035, and their importance will continue to increase as exhaust standards improve and the average vehicle weight increases (Timmers and Achten, 2016; Rexeis and Hausberger, 2009). Thus, the increasing popularity of BEVs might not trigger as significant reduction in particulate matter emissions and improvement in urban air quality as expected. However, there is little scientific evidence on how the increasing share of BEVs will in reality affect local aerosol concentrations within urban neighborhoods. To date, no studies have examined the effects of traffic fleet electrification on local aerosol concentrations at very fine resolution (a few meters) within realistic street-canyons where the highest aerosol concentrations and exceedance of the regulatory limit values are typically seen (Kiesewetter et al., 2014). This knowledge is particularly important for urban planners who design and adapt city structures to improve air quality. As an example, the City of Helsinki is redeveloping some of its access roads into boulevard-type roads surrounded by new residential neighborhoods, where good air quality is a key priority. At the same time, a substantial increase in the number of BEVs is expected in the Helsinki metropolitan region, making it essential to quantify the direct impact of the increase of BEVs on air quality at the local pedestrian level (2 m height).

This study will address this gap by examining how the increasing share of BEVs can influence aerosol concentration distributions within a planned city-boulevard on a typical winter morning. The LES PALM model system (Maronga et al., 2020) is used in the simulations, allowing a realistic representation of the characteristics of the urban surface and the dispersion of aerosols within the area of interest. We predict the fleet compositions for years 2035 and 2040 (with a base-line in year 2022) and quantify their impact on local pedestrian level aerosol number and mass concentrations in different areas (boulevard, roundabout, residential courtyards).

2 Data and methods

2.1 PALM model system

The PALM model system is used to study the dynamics of the atmospheric and oceanic boundary layer (Maronga et al., 2020). Due to its excellent scalability on massively parallel computer architectures, PALM is ideally suited for complex urban settings, which require detailed and realistic representation of atmospheric processes at fine spatial scales. PALM has a self-nesting capability (Hellsten et al., 2021) to capture the dominant turbulent eddies in the atmospheric boundary layer at the same time by resolving most of the smaller-scale kinetic energy within street canyons. In self-nesting, multiple computational domains are nested progressively at every model time step. PALM incorporates several advanced features that improve its utility for studying urban turbulence and air quality. The Cartesian topography scheme and a plant canopy model provide the aerodynamic impact of buildings and tree canopy on flow. The Sectional Aerosol module for Large Scale Applications (SALSA, Kurppa et al., 2019) simulates aerosol processes (nucleation, condensation, coagulation and dry deposition), capturing modifications to aerosol concentration and size distributions (Kokkola et al., 2008). In SALSA, the particle size distribution is discretized into

https://doi.org/10.5194/egusphere-2026-341
Preprint. Discussion started: 17 March 2026

size bins, and the chemical composition of each bin can include sulfate, organic carbon, black carbon, nitrate, ammonium, sea salt, mineral dust, and water.

The performance of the PALM model system has been extensively evaluated against wind tunnel simulations showing good agreement for mean flow and turbulence (Letzel et al., 2008; Abd Razak et al., 2013; Gronemeier and Sühring, 2019; Gronemeier et al., 2020) and scalar dispersion (Park et al., 2012) above urban-like surfaces. Similarly, multiple studies comparing PALM-SALSA with observational data have shown strong agreement, particularly in reproducing aerosol number concentrations and distributions (Kurppa et al., 2019; Du et al., 2024a).

2.2 Study area

Our study area (Figure 1) is a street located in the northwest part of Helsinki, Finland, planned to be converted to a boulevard type road surrounded by residential buildings. The planned boulevard is approximately 50 m wide with two northbound and two southbound traffic lanes (3.5 m wide each), separated by two tram lines in the middle. The outermost lanes are designated for public transport which will mainly be electric busses. On both sides, the boulevard is lined with street trees next to the roadway, followed by bike lanes and sidewalks. To the west of the boulevard there is an existing industrial area, with minor plans for new developments, while on the eastern side, residential buildings are planned to be built. Several side streets, 7 to 12 m wide, lead to parking lots and courtyards on both sides of the boulevard. At the southern end of the boulevard, a roundabout with intersecting tram lines, with buildings arranged around its circular layout. Building heights along the boulevard vary between 29 and 45 m and between 26 and 35 m at the roundabout. The estimated daily traffic volume is around 21,000 vehicles and the future estimated residential population is around 4,800.

2.3 Traffic scenarios

We consider three distinct traffic scenarios with variable amount of BEVs. Scenario 1 (S1) serves as the baseline for the year 2022, while Scenario 2 (S2) and Scenario 3 (S3) project future conditions for 2035 and 2040, respectively. The composition of the passenger car fleet in each scenario was derived from the SALAMA model (Finnish regional car fleet model; Viri et al., 2021) for the Helsinki metropolitan region. SALAMA integrates detailed individual vehicle registration data with socio-demographic information on the vehicle owner to characterize the car fleet. For urban public transport, bus fleet composition for each scenario was obtained from "GEVO 2020 - Helsinki" published by the Technical Research Center of Finland (VTT, 2018). Consequently, the modeled shares of BEVs were 10%, 60%, and 100% for scenarios S1, S2, and S3, respectively. The estimated BEV share in 2040 for scenario S3, as projected by SALAMA, was approximately 90%. However, for our calculations, we assumed a full penetration of 100% BEVs to simulate the effect of emission restrictions in the study area. The corresponding shares for battery electric busses were 15%, 30% and 55% for the three scenarios, respectively (Table 1).

The temporal and spatial distribution of traffic within the study area was predicted using a multi-layer Long Short Term Memory (LSTM) network (Leinonen et al., 2024). This deep learning based prediction method maps the traffic flow with multiple vehicle types and time steps using various non-traffic input variables (i.e. weather, accidents, and temporal attributes). The method predicts the accumulated number of each vehicle type passing a single point on the road entering our simulation

https://doi.org/10.5194/egusphere-2026-341
Preprint. Discussion started: 17 March 2026

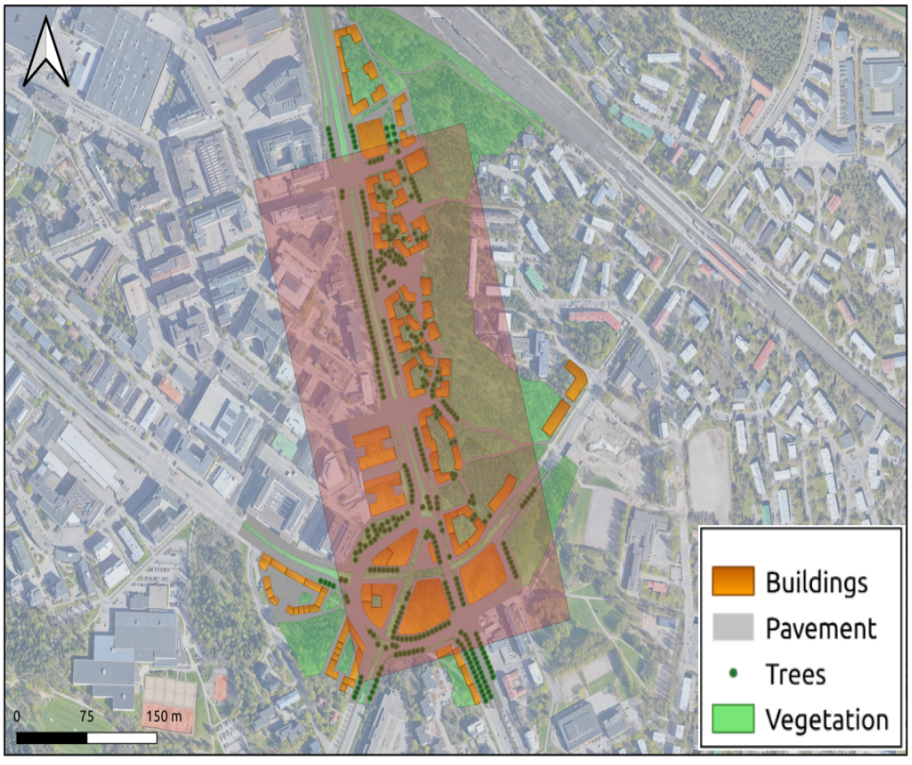

Figure 1. Map of the study area showing the child domain (red) and the proposed city boulevard (coloured blocks). The new urban layout follows the Vihdintie plan (City of Helsinki) and was integrated into the domain by the authors. Background map data: © Google Earth 2024.

area from north to south towards the center of Helsinki and vise versa, over a 15-min interval. Passenger cars represented the majority of the total vehicles, comprising 94%, while city busses and heavy-duty vehicles comprised 3% each.

During a morning rush hour on a typical January weekday from 7:00 to 9:00 (UTC+2), representing conditions similar to those used in our simulations, the total traffic rate in both directions was 1360 veh h^{-1}. Of this, 70% (952 veh h^{-1}) traveled southbound towards Helsinki city centre and 30% (408 veh h^{-1}) traveled northbound. Subsequently, traffic rate for individual street segment was calculated based on the proportion of vehicles as reported by Helsinki Region Environmental Services Authority (HSY) passing through each segment using one-hour time intervals. The boulevard speed limit is set to 40 km h^{-1}.

2.4 Model setup

2.4.1 Simulation domains and morphological data

The simulation domains consist of a root (1536 × 3072 × 64 cells), a parent (768 × 1536 × 64 cells) and a child (384 × 768 × 72 cells in the x, y and z directions) (Table 2, Figure S1). The multi-nesting approach allows airflow to be properly adjusted to the urban surface before entering the child domain, which covers our study neighborhood with a grid resolution of 1 m (Table

https://doi.org/10.5194/egusphere-2026-341
Preprint. Discussion started: 17 March 2026

Table 1. Particle number (PN) emission factors (# m^{-1}) used in this study as based on vehicle category and fleet composition estimated with the SALAMA model for three traffic scenarios for years 2022 (S1), 2035 (S2) and 2040 (S3). PC = Passenger Cars, PHEV = Plug in Hybrid Electric Vehicle, BEV = Battery Electric Vehicle, CNG = Compressed Natural Gas, HDV = Heavy Duty Vehicle.

Year	2022 (S1)		2035 (S2)		2040 (S3)	
Vehicle category	Fleet (%)	PN	Fleet (%)	PN	Fleet (%)	PN
PC (diesel, petrol, PHEV)	90	4.8×10^{10}	42	1.8×10^{10}	0.0	0.00
PC (BEV)	10	4.7×10^{8}	58	2.7×10^{9}	100	4.7×10^{9}
Bus (diesel, CNG)	85	3.8×10^{11}	70	3.1×10^{11}	45	2.2×10^{11}
Bus (BEV)	15	2.9×10^{9}	30	6.5×10^{9}	55	1.09×10^{8}
HDV (> 3.5 t)	100	6.0×10^{11}	100	6.0×10^{11}	94	5.7×10^{11}
HDV (BEV)	0.0	0.0	0.0	0.0	6	1.3×10^{9}
Total number		7.5×10^{10}		4.7×10^{10}		2.8×10^{10}

Table 2. Number of grid points (N), grid resolutions (Δ) and dimensions (L) in the x, y and z directions of the model domains used in this study.

Domain	$N_x \times N_y \times N_z$	$\Delta x \times \Delta y \times \Delta z$(m)	$L_x \times L_y \times L_z$($m^3$)
Root	1536 × 3072 × 64	9.0, 9.0, 6.0	13824×27648 × 384
Parent	768 × 1536 × 64	3.0, 3.0, 3.0	2304 ×4608 ×192
Child	384×768 × 72	1.0, 1.0, 1.0	384 × 768 × 72

2,Figure S1). The parent and root domains have a grid resolution of 3 m and 9 m, respectively. Detailed information for the root domain, including building heights, roads, land cover, trees, and orography, was obtained from a 2-m elevation model (National Land Survey of Finland, 2024). Data for the parent and child domains were obtained from high-resolution (1 m) raster maps (Strömberg et al., 2022). The newly planned area within the child domain was generated based on the Vihdintie plan provided by the City of Helsinki. This plan was integrated with the existing high-resolution data set (Figure S1). The manipulation of the input files of the domain was carried out using the Python library P4UL (Auvinen and Karttunen, 2020). The locations and heights of the existing trees within the parent and child domains were extracted from the high-resolution raster maps, while the trees in the newly developed area were manually added and assigned a uniform height of 15 m. Due to the lack of observational data on tree leaf area density (LAD), a constant LAD value was applied to all tree crowns above z_{min}= 4m. The street trees in Helsinki are predominantly broadleaf species such as lime trees (Tilia); therefore, winter LAD values were estimated to be 80% smaller (0.2 m^2 m^{-3}) than the summer value of 1.2 m^2 m^{-3} for broadleaf trees (Abhijith et al., 2017). The trees in parks and forested areas are a mixture of broadleaf and evergreen trees; therefore, a 60% decrease (0.5 m^2 m^{-3}) in the LAD values was applied for the winter.

https://doi.org/10.5194/egusphere-2026-341
Preprint. Discussion started: 17 March 2026

2.4.2 Meteorological boundary conditions

The dynamic meteorological boundary conditions were obtained from the MetCoOp Ensemble Prediction System (MEPS; Müller et al., 2017). MEPS has a horizontal resolution of 2.5 km, 65 vertical levels, and 30 ensemble members. It is run four times per day (i.e., at 00:00, 06:00, 12:00, and 18:00 UTC) with a 3-hour cycle for data assimilation (3D-Var). MEPS uses the European Center for Medium-Range Forecasts (ECMWF) as its lateral boundary model and produces model output every hour. The MEPS data were downloaded from the data archive (Norwegian Meteorological Institute, 2021) using the File Interpolation, Manipulation, and Extraction (Fimex) library (Norwegian Meteorological Institute) for the ensemble member 0 (i.e., the control member) without perturbations to the initial or boundary conditions.

The initial conditions and dynamic meteorological boundary data were provided to PALM by a dynamic driver. The dynamic driver was created using a Python script (Kurppa and Strömberg, 2020) using the following procedure. First, the sigma levels were translated into pressure levels and then into height levels by applying the hypsometric equation. Then, u, v, w, potential temperature (θ) and the water vapor mixing ratio were horizontally and vertically interpolated from the MEPS grid to the PALM grid within the root domain using the cubic spline and linear interpolation methods, respectively. The mean potential temperature over our simulation period indicates a relatively weak or neutral stable boundary layer (Figure S2).

2.4.3 Air pollutant emissions

Air pollution emissions from road traffic are considered only within the child domain. The emission factors (EFs) of $PM_{2.5}$ from both exhaust and non-exhaust emissions were calculated from The Handbook of Emission Factors for Road Transport (HBEFA; Notter et al., 2022). HBEFA provides regularly updated emission data for all common vehicle categories, traffic situations, technologies, and emission standards from 1990 to approximately 2050 for six European countries. Since Finland is not included in the HBEFA emission data set, the EFs for Sweden were used in this study. As a first step, the number EFs of the speed limit (40 km h^{-1}) were calculated for various vehicle categories and fuel technologies in the free-flow traffic scenario for winter. The EFs were then weighted based on the vehicle fleet compositions (Table 1) for the three traffic scenarios. In SALSA, particle number size distributions are used to define how the total concentration of aerosol number is partitioned into discrete size bins (10 in our case). Consequently, three particle size distributions corresponding to years 2022, 2035 and 2040 were used (Figure 2). For S1 (2022), the size distribution reported by Hietikko et al. (2018) was used. For S2 (2035) and S3 (2040), the size distributions were derived using the baseline distribution (S1), with the number of particles adjusted according to the reductions in total EF (Table 1). Accordingly, the total number of emission factors of $EF_N = 7.5 \times 10^{10}$ # m^{-1}, $EF_N = 4.7 \times 10^{10}$ # m^{-1}, and $EF_N = 2.8 \times 10^{10}$ # m^{-1} were applied for S1, S2 and S3, respectively (Table 1).

The final particle emissions are introduced into PALM-SALSA as dynamic surface fluxes (in # m^{-2} s^{-1}) within the child domain (Figure 3). These were calculated hourly according to:

$$\text{Particle emission flux} = EF \times \left(\frac{\text{traffic rate}}{\text{street length/ total road surface area}} \right) \times 3600(\text{s}). \quad (1)$$

https://doi.org/10.5194/egusphere-2026-341
Preprint. Discussion started: 17 March 2026

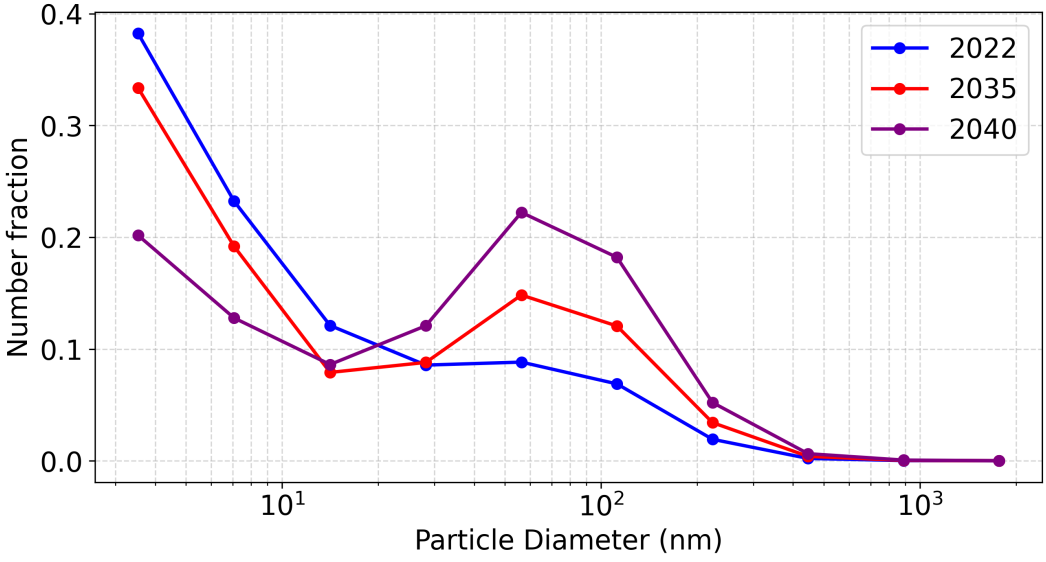

Figure 2. Input particle number size distribution base on number fraction of aerosol size bins in the boulevard for three traffic scenarios, S1 (2022), S2 (2035), and S3 (2040).

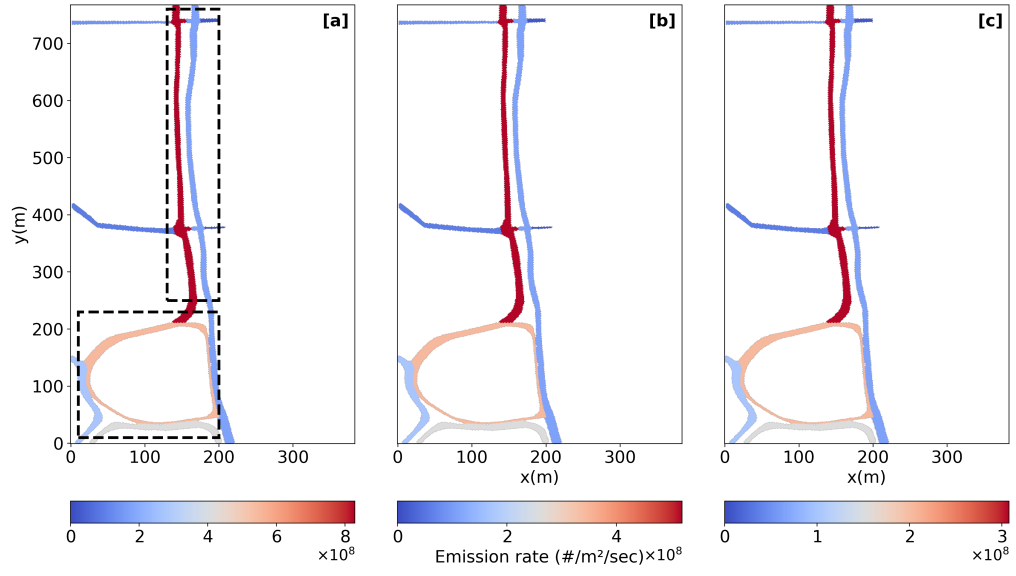

Figure 3. Hourly aerosol emission maps (in # m^{-2} s^{-1}) for the child domain from 8:00 to 9:00 are shown for the three scenarios: (a) S1 (2022), (b) S2 (2035), and (c) S3 (2040). The black dashed boxes in (a) show the selected statistical regions representing the boulevard (SR1, upper box) and the roundabout (SR2, lower box).

https://doi.org/10.5194/egusphere-2026-341
Preprint. Discussion started: 17 March 2026

2.4.4 Model runs and initialization

This study used the PALM model system version 23.10 together with the SALSA aerosol module to simulate aerosol number and mass concentrations and their size distributions. Simulations were performed for the winter morning rush hour from 7:00 to 9:00 UTC+2 with meteorological conditions from January 15 2021. The simulation time was further divided into spin-up (7:00-8:00 UTC+2) and main run (8:00-9:00 UTC+2 (Figure 4). Meteorological data are provided to the model at an hourly resolution. During the simulation, the mean air temperature was -21.6°C and the mean wind speed 3.9 m s^{-1}. The prevailing wind direction was North-Northeast, which is nearly parallel to the planned city boulevard (Figure 4). As the simulation took place before sunrise, no thermal turbulence due to solar radiation was considered. In our simulation, the stability of the boundary layer is determined by the vertical potential structure - provided by the MEPS data used in the dynamic input file. During the run, PALM continuously updates the potential temperature at all lateral and top boundaries based on the dynamic forcing fields varying over time. Furthermore, vehicle-induced turbulence was not considered due to the comparative nature of the study with the same traffic rates used in each scenario.

The parent and child domains were nested by using one-way self nesting. Due to its high computational demands, SALSA was applied only within the child domain. The aerosol particle size distribution was described using 10 size bins within two subranges: three size bins within the first subrange (2.5–20 nm) and seven bins within the second subrange (20 nm–2.5 μm). From the aerosol process, only dry deposition was considered and calculated every 1 s. Coagulation was ignored due to its minimal impact on aerosol dynamics and high computational cost (Kurppa et al., 2018b). Similarly, condensation can be neglected because the timescale for condensation is longer than the duration that air remains within the street canyon (). As SALSA was run only within the child domain, nesting was not applied for pollutant concentrations, and air pollutants boundary conditions were set at the child domain boundaries. We conducted simulations both with and without aerosol background concentration included. We focus only on the latter, as our primary interest is to assess the impact of changing traffic emissions due to vehicle fleet electrification on aerosol concentrations, while background concentrations, particularly in future scenarios in 2035 (S2) and 2040 (S3) remain uncertain.

The outputs for both the root and parent domains, including 4D spatial and temporal averaging, cross sections, and flow field profiles (u, v, w) and θ, were saved at 10-minute intervals with spatial resolutions of 9 m and 3 m, respectively, after the first 10-min of the main run leaving 50-min for data analysis. In addition, for the child domain, aerosol concentrations were saved. The variables analyzed included concentrations of $PM_{2.5}$, $PN_{2.5}$, UFP (ultrafine particles, diameter < 100 nm) and size distribution. The variables were saved with higher temporal (2-minute) and spatial (1 m) resolutions. We evaluate results within the whole child domain and separately within the main street and the roundabout. The boulevard refers to the statistical region SR1, and the roundabout corresponds to the statistical region SR2 (Figure 3). The statistical regions cover areas of 190×220 m and 60×510 m, respectively, extending from ground level to a height of 72 m. Simulations were performed on the Center for Scientific Computing (CSC) Mahti supercomputer. Using in total 648 Intel Xeon processor cores, each simulation required 72 hours of computing time.

https://doi.org/10.5194/egusphere-2026-341
Preprint. Discussion started: 17 March 2026

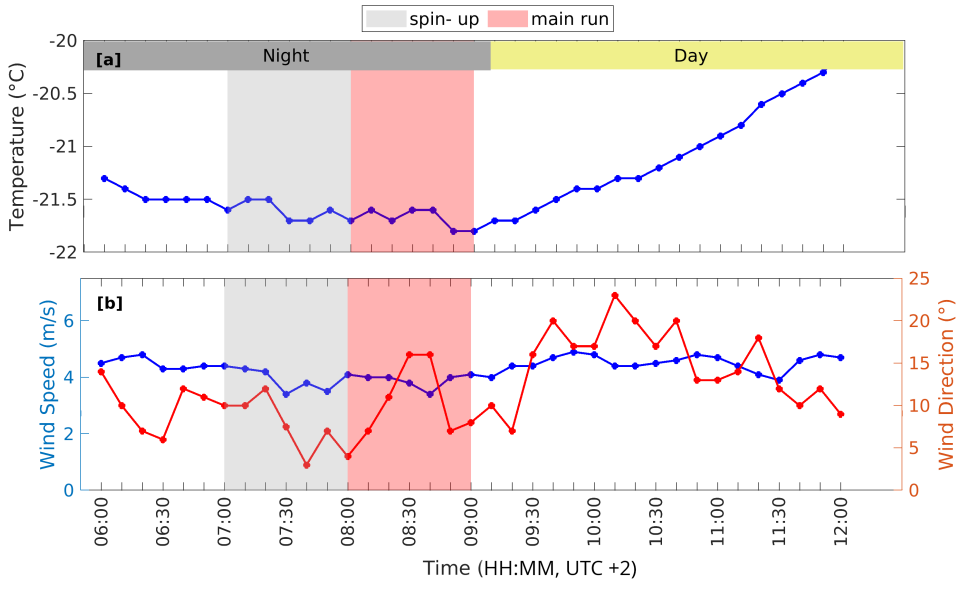

Figure 4. 10-min meteorological variables of a) air temperature and b) wind speed and direction during the day of the simulation (January 15 2021) as measured at the Finnish Meteorological Institute weather station located in Kumpula about 4.7 km from the child domain. The gray area highlights the spin-up run from 7:00 to 8:00, and red the main run from 8:00 to 9:00. Night and Day refer to times before and after the sunrise, respectively.

3 Results and discussion

3.1 Time-averaged wind flow fields

The mean horizontal wind speeds within the child domain at three heights (2 m, 10 m, and 20 m) are illustrated in Figure 5. Note that the flow fields are shown only for S2, as all the scenarios used the same meteorological forcing. The mean wind speed within the child domain at a height of 2 m is 0.9 m s^{-1}. The flow is strongly influenced by the arrangement of buildings and streets, as well as by the presence of short vegetation, particularly on the right-hand side of the domain. In general, low vegetation reduces wind speeds. This is consistent with previous studies, which found that low vegetation tends to decelerate air flow (Du et al., 2024b; Shen et al., 2023). Along the boulevard and around the roundabout, the mean wind speeds increase to approximately 1.0 m s^{-1}. The highest wind speeds, up to 3.5 m s^{-1}, occur in the northern section of the boulevard where vegetation is absent, near the cross-section in the middle-left part of the domain, and in the southern part of the domain. The latter is attributed to the channeling effects between the buildings located on the right side of the boulevard and those around the roundabout. The average wind speed within the child domain increased by 30% (1.2 m s^{-1}) and 56% (1.6 m s^{-1}) at heights of 10 m (Fig. 4b) and 20 m (Fig. 4c), respectively, relative to the near-surface wind at 2 m, due to the reduced influence of obstacles. However, in some sections of the tree-lined boulevard and within the courtyards on the right-hand side of the domain,

https://doi.org/10.5194/egusphere-2026-341
Preprint. Discussion started: 17 March 2026

local wind speeds at 10 m are lower than at 2 m. This is due to the effect of the tree canopies on the flow. In our simulations, the tree canopy extends from approximately 4 to 15 m above ground level (see Fig. 2 for tree locations). Consequently, the canopy's sheltering effect in reducing wind speed is clearly evident at a height of 10 m. This aligns with the study by (Du et al., 2024b) in a busy crossroad in Malmö, Sweden. Above the building canopy (beyond 40 m, not shown), the flow becomes more homogeneous and moves more freely due to the absence of roughness elements (e.g. buildings, trees). The wind direction there largely follows the prevailing north-northwest flow. In contrast, within the urban roughness sublayer, where the atmosphere is directly shaped by roughness elements, flow and transport are highly complex and heterogeneous because of the interaction between turbulence and the varied arrangement and morphology of these elements (Auvinen et al., 2020; Cheng et al., 2021; Torres et al., 2021).

To understand vertical flow conditions, a vertical representation of the average w along the boulevard (SR1, Figure 6a) and the roundabout (SR2, Figure 6b) is plotted. The average vertical wind speeds are notably low, only -0.01 m s^{-1} on the boulevard and 0.04 m s^{-1} on the roundabout. The buildings also shape the distribution of w and even buildings less than 15 m in height cause the flow to deflect upward creating vortices in which w reaches 1.2 m s^{-1}. That is consistent with the classical description of flow separation and vortices of the recirculating cavity behind obstacles mounted on the surface (Hunt et al., 1978). In Figure 5a, the 32 m building on the left side of the domain generates a pronounced wake structure characterized by a strong upward flow along its windward face, a downward flow immediately downstream on the leeward side, and a clearly defined recirculation bubble in the near wake. Within this recirculation region, upward vertical velocities reach magnitudes of approximately 1.0 m s^{-1}. These features demonstrate that our simulation accurately captures the characteristic wake-recirculation dynamics behind high-rise buildings, consistent with experimental studies and LES and wind tunnel models showing that tall structures strongly govern the flow pattern within the urban roughness sublayer (Mishra et al., 2024; Akinlabi et al., 2022; Hertwig et al., 2019).

https://doi.org/10.5194/egusphere-2026-341
Preprint. Discussion started: 17 March 2026

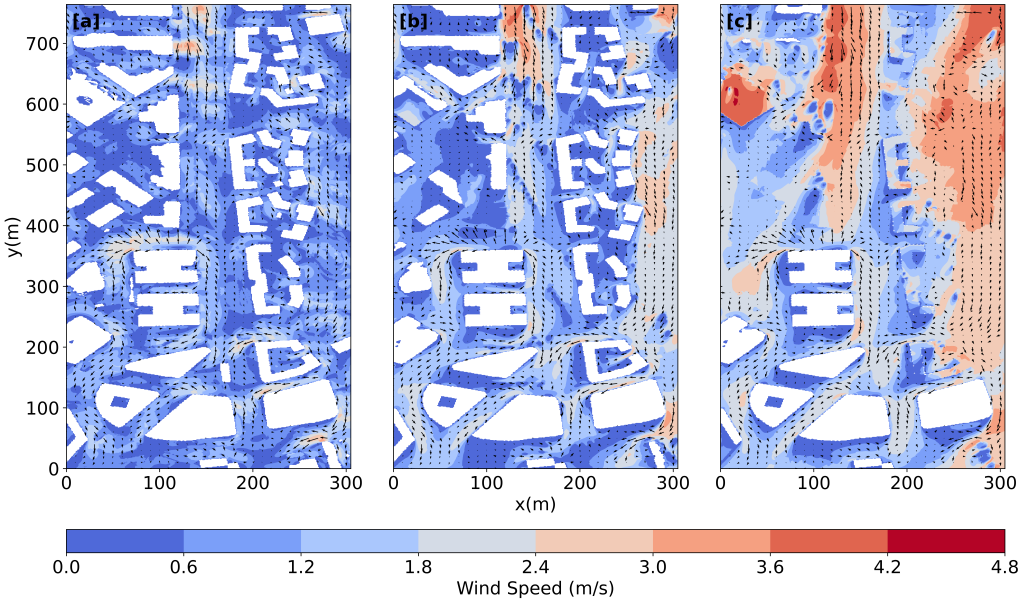

Figure 5. Mean horizontal wind speed for the child domain at 2-m (a), 10-m (b), and 20-m (c) height between 08:00 and 09:00 in 2035 corresponding scenario S2 using meteorological data from 15 January 2020. Black arrows show direction of the flow.

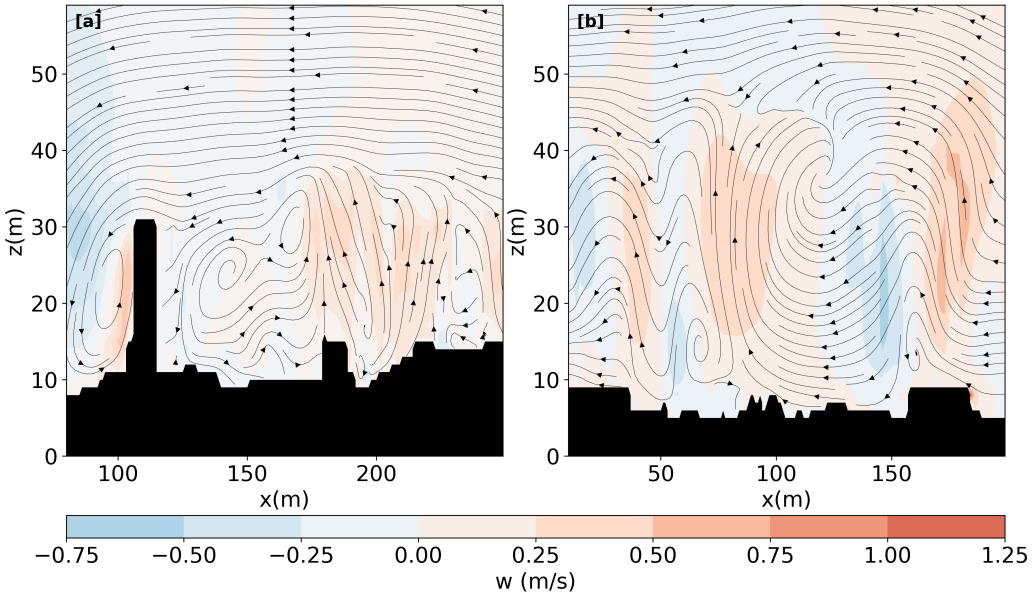

Figure 6. Vertical mean wind (w) averaged along the boulevard (a) and the roundabout (b). The streamlines describe the flow rotating around the y-axis aligned with the street and the colors describe the vertical wind speed. Black areas represent buildings on both sides of the street.

https://doi.org/10.5194/egusphere-2026-341
Preprint. Discussion started: 17 March 2026

3.2 Aerosol particle number and mass concentration in different traffic scenarios

The mean spatial variabilities of $PN_{2.5}$ at the near-surface level in the different scenarios are shown in Figure 7. In S1, a mean concentration of 1800 cm^{-3} is seen (Figure 7a). Higher concentrations are observed on the western side of the main road with higher traffic rates towards the city center during the morning rush hour. The highest pollutant concentrations, exceeding 12,300 cm^{-3}, are observed in two distinct hotspots on the left side of the boulevard. The first occurs near a building corner interfacing with the open boulevard, where traffic splits between the city center and the west. The second hotspot is located at the intersection of the boulevard and the roundabout. The elevated concentrations observed here correspond to the development of aerodynamic stagnation zones induced by building geometries, which significantly restrict the advective dispersion. These observations are supported by recent LES research highlighting the critical role of building's geometry in altering pollutant transport mechanisms (Zheng et al., 2022; Hassan et al., 2022). On average, $PN_{2.5}$ in the boulevard and roundabout is 3400 cm^{-3} and 3600 cm^{-3}, respectively (Figure 9). Concentrations decrease rapidly in side streets and courtyards, mainly due to the canyon effect on flow, which restricts the dispersion and transport of pollutants away from emission sources (Xie et al., 2005; Yazid et al., 2014; Zhang et al., 2020). The lower modeled concentrations can be attributed to the omission of background particle levels from our simulations, which would otherwise increase the predicted values. In a separate model run that included background concentrations (not shown), the average hourly $PN_{2.5}$ concentration reached 20,000 cm^{-3}, substantially exceeding the contribution from traffic emissions within the boulevard. This occurs because, during winter in Helsinki, the urban background is strongly influenced by residential wood combustion and long-range transported pollution, which can become trapped under frequent thermal inversions (Teinilä et al., 2024). Consequently, the air entering the street canyon is already heavily loaded with particles, so the additional increase from local traffic appears relatively modest in time-averaged statistics. These findings are consistent with a wintertime street-canyon measurement campaign conducted in Helsinki (January–February 2022) by Teinilä et al. (2019), which reported an average $PN_{2.5}$ concentration of 19,900 cm^{-3} under slightly lower traffic conditions (1192 veh/h) than those used in our simulation (1358 veh/h). The spatial distribution of $PN_{2.5}$ at 2-m height remains consistent across all scenarios due to identical meteorological conditions (Figure 7). However, there are notable variations in the concentration magnitudes between scenarios (Figure 9) due to the different amount of BEVs within the traffic fleet. The average $PN_{2.5}$ within the child domain decreases by 37% (353 cm^{-3}) in S2 and by 62% (211 cm^{-3}) in S3, compared to the baseline reflecting direct reductions in total EF (Table 1). In the boulevard, the reductions are nearly the same, 38% to 62% for S2 and S3, respectively. In the roundabout, the reductions are slightly smaller, 34% to 62% for S1 and S2, respectively, compared to the baseline. In particular, the reduction is most significant for the UFPs fraction (< 0.1 μm), with concentrations decreasing by 42% in S2 and 68% in S3 (Figure S3). This disproportionate reduction aligns with the established literature on traffic aerosols: internal combustion engines are the primary source of nucleation and Aitken mode particles (Rönkkö and Timonen, 2019; Pirjola et al., 2019). By transitioning to BEVs, tailpipe emissions are eliminated, thereby eliminating the dominant source of high-number-count UFPs, while non-exhaust emissions continue to contribute to larger particle modes (Beddows and Harrison, 2021).

https://doi.org/10.5194/egusphere-2026-341
Preprint. Discussion started: 17 March 2026

The spatial distribution of $PM_{2.5}$ closely follows that of $PN_{2.5}$ (Figure 8). Within the child domain, $PM_{2.5}$ concentrations average approximately 2 μg m^{-3}, whereas along the boulevard and at the roundabout they range from 3 to 11 μg m^{-3} (Figure 9). Similar to $PN_{2.5}$, our simulated $PM_{2.5}$ levels are slightly lower than reported values, mainly due to the absence of the urban background in the model setup. When the background is included, the average $PM_{2.5}$ concentration is about 17 μg m^{-3}, indicating that the background contribution plays a crucial spatial role in winter for both number and mass concentrations.

Our simulation results agree well with the findings of Teinilä et al. (2019), who reported winter 2022 $PM_{2.5}$ concentrations of 3–11 μg m^{-3} in a Helsinki street canyon. They are also consistent with earlier winter morning rush-hour measurements at urban sites in Helsinki, which indicate higher $PM_{2.5}$ levels, typically 15–23 μg m^{-3} (Teinilä et al., 2019; Helin et al., 2018).

Unlike the number of concentrations, the mass concentrations increase in the future scenarios S2 and S3 compared to the baseline. The average $PM_{2.5}$ increases by 7% and 15%, respectively, within the child domain. This is consistent with Beddows and Harrison (2021), who reported a 21% increase in particulate mass due to fleet electrification. Using a weight-dependent emission model, they attributed this increase to the increased curb weight of BEVs, the heavier battery mass generates higher tire and road abrasion forces, effectively compensating for the reduction in brake dust gained from regenerative braking (Timmers and Achten, 2016; Liu et al., 2021; Piscitello et al., 2021; Fussell et al., 2022).

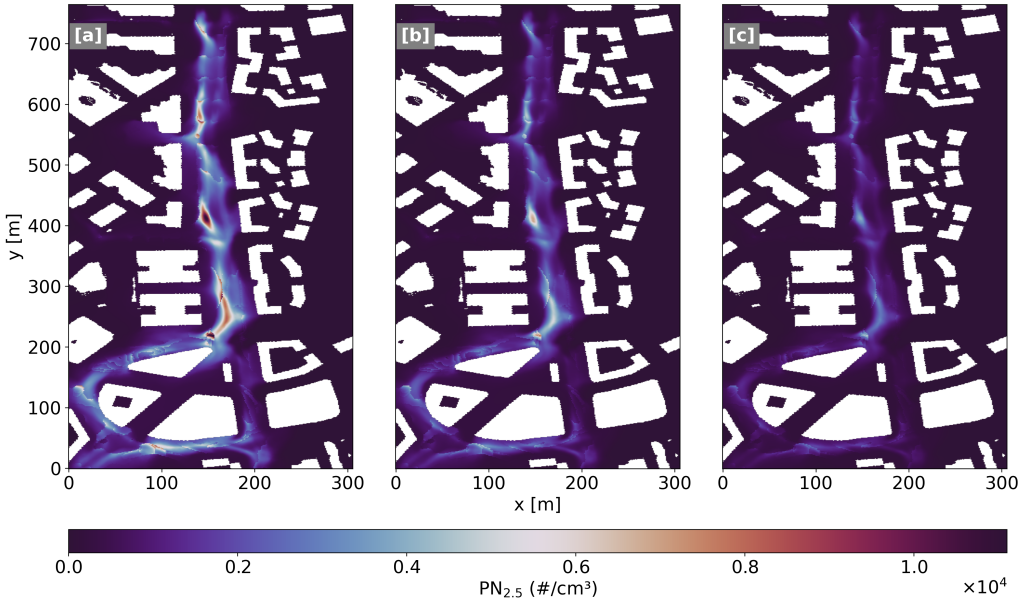

Figure 7. Mean $PN_{2.5}$ concentration (# cm^{-3}) for (a) the baseline scenario (S1), (b) S2 (2035), and (c) S3 (2040) at $z = 2$ m as calculated from 08:00 to 09:00.

https://doi.org/10.5194/egusphere-2026-341
Preprint. Discussion started: 17 March 2026

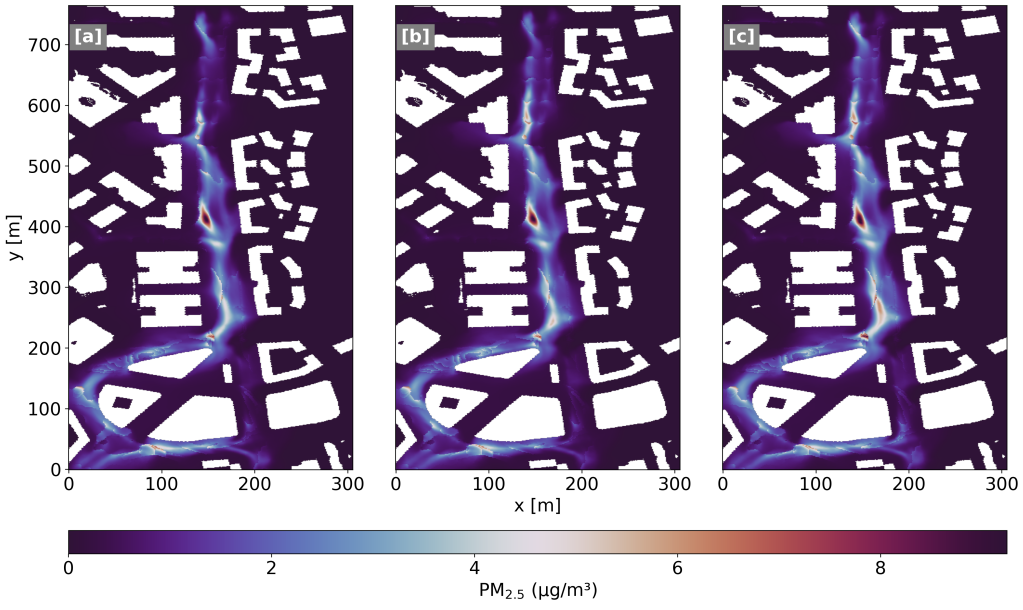

Figure 8. Mean $PM_{2.5}$ concentration (# cm^{-3}) for (a) the baseline scenario (S1), (b) S2 (2035), and (c) S3 (2040) at $z = 2$ m as calculated from 08:00 to 09:00.

https://doi.org/10.5194/egusphere-2026-341
Preprint. Discussion started: 17 March 2026

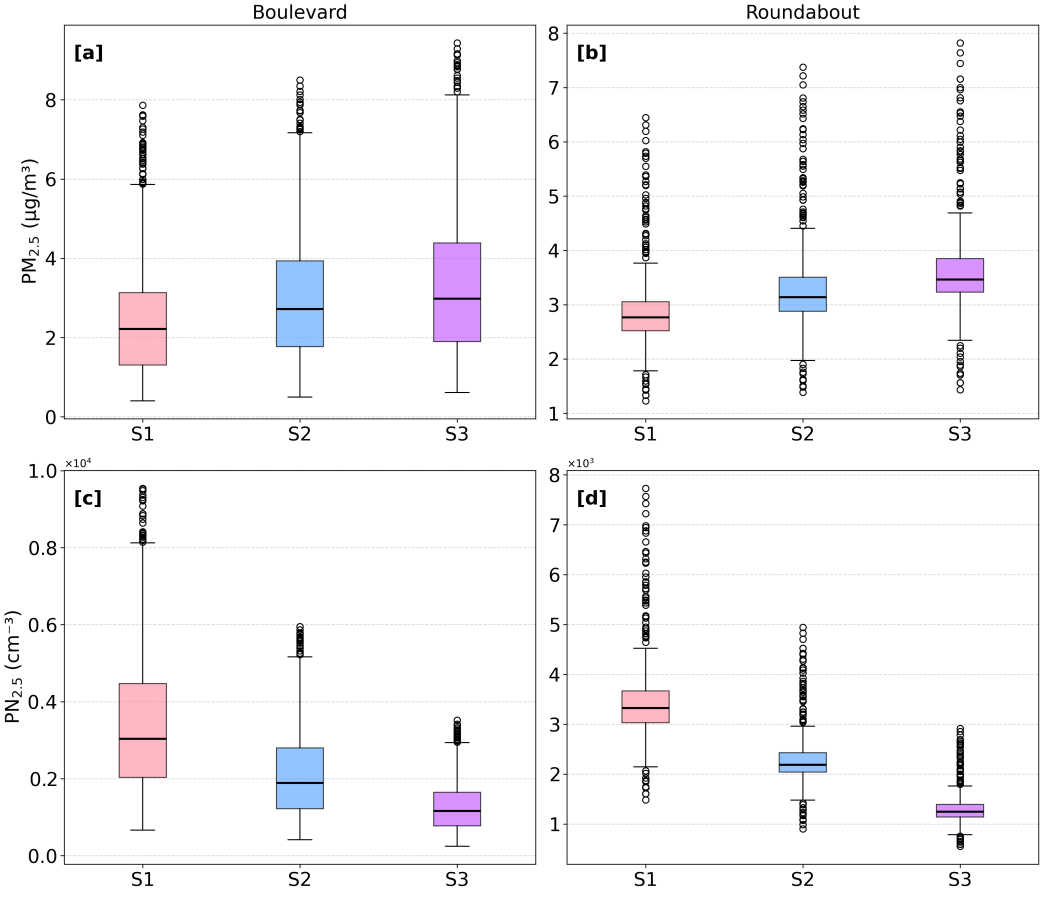

Figure 9. Fine particle mass concentrations ($PM_{2.5}$, $\mu g\ m^{-3}$) and number concentration ($PN_{2.5}$, m^{-3}) at 2 m height on the (a,c) boulevard (SR1) and (b,d) roundabout (SR2) during 08:00 - 09:00 for the baseline (S1), scenario S2 (2035), and scenario S3 (2040). Black lines show the median values, the box represents the 25th and 75th percentiles, and the whiskers represent the 95th percentiles.

3.3 Vertical profile of particle number concentrations

The mean vertical profiles of $PN_{2.5}$ on both sides of the boulevard and at the roundabout are illustrated in Figure 10. At all three locations, the average vertical profiles show a pronounced reduction in $PN_{2.5}$ concentrations near the surface, up to approximately 10 m, in all scenarios. Such a rapid decrease is commonly observed in street canyons due to reduced vertical mixing and dispersion of pollutants (Järvi et al., 2023). This near-surface reduction is approximately 82%, 88%, and 52% at the roundabout, and on the western and eastern sides of the boulevard, respectively. Above this height, the vertical profile remains relatively constant up to about 35 m, corresponding to the average building canopy height. A secondary, gradual reduction is observed as the profiles extend above the building canopy (Figure 10).

Among the three locations, the eastern part of the boulevard (Figure 10c) shows the lowest average reduction (52%) in aerosol concentration from the surface up to 10 m compared to the roundabout and the western side (Figure 10a,b). This can be

https://doi.org/10.5194/egusphere-2026-341
Preprint. Discussion started: 17 March 2026

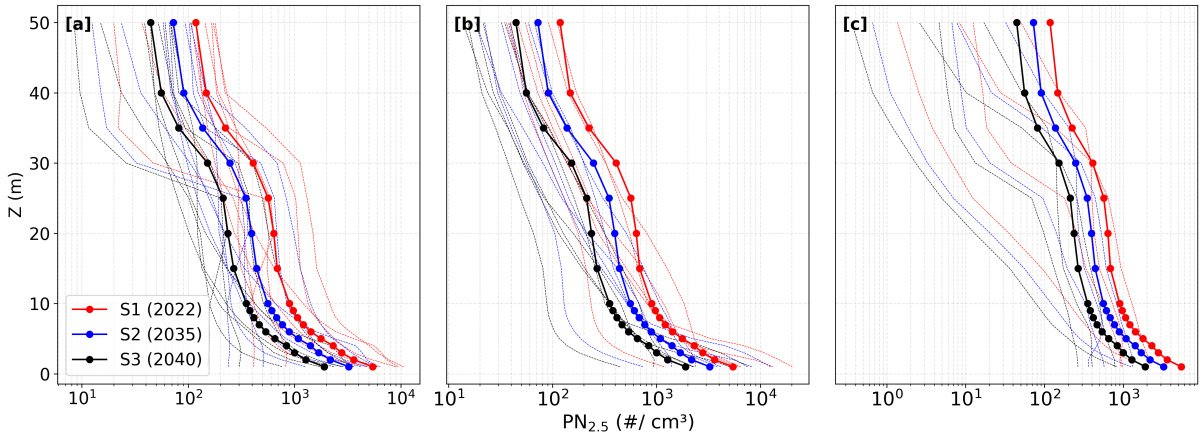

Figure 10. The geometric vertical profiles of total particle number concentration ($PN_{2.5}$, # cm^{-3}) at the roundabout (a), the western side (b), and the eastern side (c) of the boulevard. Gray lines depict the vertical profiles for various spots across all scenarios, while the solid lines with markers indicate the mean vertical profiles of selected spots for the baseline scenario S1 (2022) and the future scenarios S2 (2035) and S3 (2040).

attributed to the local wind field: the eastern part lies slightly on the leeward side, where the horizontal wind speed is lower near the surface (Figure 5), leading to reduced ventilation and, consequently, a smaller reduction in $PN_{2.5}$ with height. In contrast, stronger wind flow at the roundabout and on the western side enhances the rapid dilution and dispersion of pollutants as they ascend (Yassin and Ohba, 2012).

Dry deposition onto vegetation and trees may also contribute to near-surface particle removal. In SALSA, dry deposition is parameterized as a particle-size-dependent process that accounts for Brownian diffusion, turbulent impaction, and gravitational settling, which together determine the deposition velocity for each aerosol size bin.

However, when examining individual vertical profiles next to the buildings and between the tall buildings at the roundabout, a different behavior from the average profiles emerges. At these locations, concentrations remain relatively constant up to the building canopy height before showing a gradual decrease. In these street-canyon configurations, characterized by tall buildings and narrow gaps between them, vertical dispersion is slower, resulting in a more gradual reduction in concentrations with height. These findings are consistent with Yassin and Ohba (2012); Gromke and Ruck (2012), who report a clear relationship between concentration levels and the street-canyon aspect ratio.

In all scenarios, pollutant concentrations decrease with height and with distance from the street, as road traffic is the dominant emission source in our simulations. Furthermore, the modeled period corresponds to a stable, cold winter morning, which limits vertical mixing (Uehara et al., 2000). This reduces ventilation and allows pollutants to persist near the street and to accumulate on nearby surfaces and vegetation, leading to higher concentrations close to the ground.

https://doi.org/10.5194/egusphere-2026-341
Preprint. Discussion started: 17 March 2026

3.4 Aerosol particle number size distribution

To illustrate the influence of aerosol dynamic processes on particles of different sizes, the modeled particle number size distributions at 2 m height on the boulevard are presented in Figure 11. As seen already in $PN_{2.5}$, the particle size distributions also exhibit a pronounced decrease in particle concentrations from S1 to S2 and S3. Largest reductions are seen in the UFP range (<50 nm), as seen already in their spatial patterns. In S2 , when around 60% of the vehicle fleet is assumed to be BEVs, the concentrations in the smallest bins drop by roughly 40–60%, from 2200 to 1270 cm^{-3} at 4 nm and from 1350 to 735 cm^{-3} at 9 nm. By 2040, when passenger cars are fully electrified (S3), concentrations decline further by about 80% from 2200 to 430 cm^{-3} at 4 nm relative to S1. In the accumulation mode (100–300 nm), the reductions are more moderate, typically 20–50%, from 525 to 400 cm^{-3} at 160 nm, indicating that the coarse and secondary aerosol sources remain relatively stable. For the largest particles (>500 nm), changes are small in absolute terms but still show a gradual downward trend (from 12.9 to 14.1 cm^{-3} at 544 nm and 1.15 to 1.46 cm^{-3} at 1000 nm). These trends suggest that, while vehicle electrification effectively reduces UFP emissions, dry deposition increasingly contributes to the removal of larger particles near the surface. In general, the temporal evolution of particle number size distributions reflects the impacts of both the transition to BEVs and the physical removal processes that will lead to cleaner urban air by 2040.

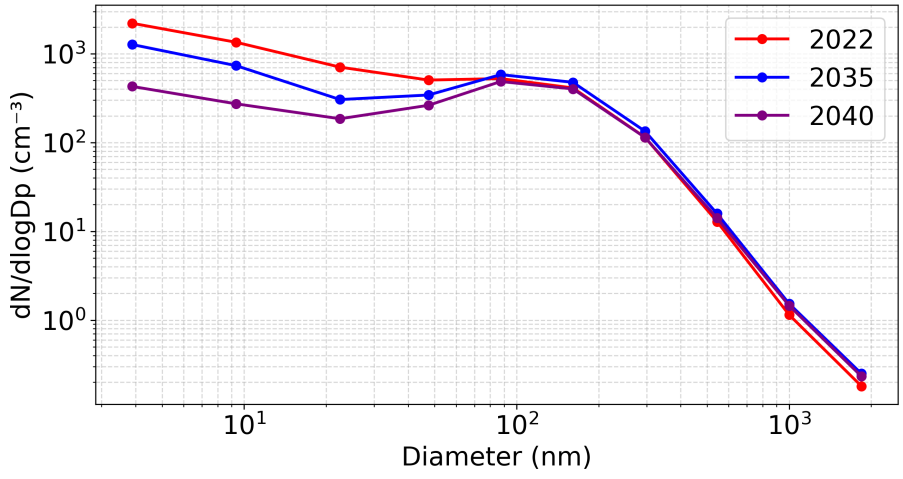

Figure 11. Particle number size distributions (PSD) within the boulevard at $z = 2$ m for three traffic scenarios, S1 (2022), S2 (2035), and S3 (2040)

3.5 Study Limitations

This study focused on a cold winter morning during a rush hour period with a neutral/slightly stable atmosphere (Figure S2). Stable atmospheric conditions remain a challenge in LES, particularly when modeling air quality in poorly ventilated urban canyons. In such environments, the lack of properly resolved turbulent eddies can lead to unrealistic spatial predictions of pollutant concentrations (Resler et al., 2024). However, since our case was only mildly stable, the related uncertainties are

https://doi.org/10.5194/egusphere-2026-341
Preprint. Discussion started: 17 March 2026

expected to be small. Also, since the meteorological conditions were identical in all our scenarios, the possible uncertainties do not affect the comparative results, but rather the spatial variability of the flow field and aerosol concentrations.

In our simulation we did not consider vehicle induced turbulence. This has been shown to strongly affect freshly emitted pollutants near the surface in regional air quality models (Makar et al., 2021). In our case the effect of vehicle induced turbulence on modeled concentrations is likely smaller as Resler et al. (2024) reported how the impact of vehicle induced turbulence on aerosol concentrations is limited when the wind speed exceeds 1.2 m s^{-1}, which is much lower than our mean wind (3.9 m s^{-1}). Furthermore, we excluded the aerosol background because of uncertainties in its magnitude in future cases and because the focus here was on local traffic emissions. Neglecting the background will impact aerosol processes and thus have some minor impact on our comparative results. However, we did not change the general conclusions. Simulating future scenarios also required other assumptions, particularly regarding the particle size distributions emitted by BEVs, which introduce some uncertainty into the model predictions.

4 Conclusions

This study examines how an increasing share of battery electric vehicles (BEVs) potentially affects aerosol number and mass concentrations and aerosol size distribution along a planned boulevard in Helsinki using the PALM model system. Three traffic fleet scenarios are simulated: S1 (2022) represents the baseline scenario, and S2 (2035) and S3 (2040) project future conditions with BEV shares of 10%, 60% and 100%, respectively. Similarly, the proportion of battery electric buses is modeled at 15%, 30%, and 55% in the three scenarios. All traffic scenarios are simulated for a cold winter morning rush hour (7:00 to 9:00 am, local time). The model setup consists of three domains, root, parent, and child with spatial resolutions of 9, 3 and 1 m. The aerosol module SALSA is applied only within the child domain which covers our area of interest where a current highway corridor is planned to be converted to a boulevard type road.

Based on our simulations, $PN_{2.5}$ concentrations are projected to decline under future scenarios with an increasing share of BEVs. The average near-surface (2 m height) $PN_{2.5}$ within the study area is 1440 cm^{-3} for the baseline scenario, but decreases by approximately 40% in S2 and 60% in S3. In contrast to $PN_{2.5}$, $PM_{2.5}$ levels are projected to increase in the coming decades, with average concentrations increasing by 7% in 2035 (S2) and 15% in 2040 (S3) from baseline. Changes in concentration are reflected in local particle size distributions. The number of ultrafine particles (<50 nm) decreases by up to 80% with increasing share of BEV within the boulevard, while accumulation-mode particles (100–300 nm) show a moderate 20–50% reduction, and coarse particles (>500 nm) remain largely unchanged in the number size distribution, but naturally have larger mass. The local topography and building layout greatly affect the flow field and the aerosol concentration distributions. The mean vertical profiles show a strong decrease in $PN_{2.5}$ concentrations within the first 10 m above ground at all locations, followed by nearly constant values up to the building canopy height and a gradual reduction above it. The magnitude of the near-surface reduction varies spatially (from 52% to 88%), with the smallest decrease (50%) on the eastern side of the boulevard, likely due to weaker ventilation under leeward wind conditions. Overall, limited vertical mixing during stable winter conditions and street-canyon geometry govern the persistence of elevated particle concentrations close to the street.

https://doi.org/10.5194/egusphere-2026-341
Preprint. Discussion started: 17 March 2026

The results show how the increasing share of BEVs will reduce tailpipe exhaust emissions and local aerosol number concentrations in urban areas. However, their larger size and weight contribute to a substantial increase in non-exhaust emissions, including brake and tire wear, which increases $PM_{2.5}$ levels. This demonstrates how the effect of cleaner technologies is not straightforward on local air quality due to non-linearities and changes in the emission aerosol size distributions. The results also provide future levels of aerosol particles in an urban future neighborhood providing scientific insights on the locations of hotspots and the accumulation of pollutants, which is important information for urban planners. To our knowledge, this is the first time the potential effect of BEVs on local aerosol concentrations is examined in a real neighborhood with realistic changes in emission scenarios, thus providing more detailed information on the possible changes in future aerosol particle concentrations.

Code and data availability.

All the input data and data processing python scripts used in this work can be accessed by contacting the authors.

https://doi.org/10.5194/egusphere-2026-341
Preprint. Discussion started: 17 March 2026

Appendix A: Particle concentration statistics

Table A1. Statistical analysis (mean, median, 5th and 95th percentiles) of fine particle number concentration ($PN_{2.5}$, cm^{-3}) and mass concentrations ($PM_{2.5}$, $\mu g\ m^{-3}$) at $z = 2$ m for the entire child domain, the boulevard, and the roundabout and three traffic scenarios. Scenario S1 represents the baseline for 2022, while S2 and S3 represent future scenarios for 2035 and 2040, respectively.

	Child domain					
Scenario	S1		S2		S3	
Variables	N_{tot}	PM $_{2.5}$	N_{tot}	PM $_{2.5}$	N_{tot}	PM $_{2.5}$
Mean	1.8×10^3	3.1	1.13×10^3	3.3	6.7×10^2	3.6
Median	1.35×10^3	2.7	8.5×10^2	2.9	1.2×10^3	3.0
5th percentile	1.4×10^3	2.0	1.7×10^1	2.0	1.25×10^1	2.1
95th percentile	5.4×10^3	5.4	3.4×10^3	5.7	4.9×10^3	6.5
	boulevard					
Scenario	S1		S2		S3	
Variables	N_{tot}	PM $_{2.5}$	N_{tot}	PM $_{2.5}$	N_{tot}	PM $_{2.5}$
Mean	3.4×10^3	3.3	2.1×10^3	3.7	1.3×10^3	4.0
Median	3.0×10^3	3.0	1.9×10^3	3.4	1.1×10^3	3.7
5th percentile	1.1×10^3	2.0	7.0×10^2	2.1	4.3×10^2	2.1
95th percentile	7.0×10^3	5.6	4.3×10^3	6.1	3.5×10^3	7.0
	Roundabout					
Scenario	S1		S2		S3	
Variables	N_{tot}	PM $_{2.5}$	N_{tot}	PM $_{2.5}$	N_{tot}	PM $_{2.5}$
Mean	3.6×10^3	3	2.4×10^3	3.5	1.4×10^3	3.8
Median	3.3×10^3	2.8	2.1×10^3	3.1	1.3×10^3	3.5
5th percentile	2.5×10^3	2.3	1.6×10^3	2.6	9.3×10^2	2.8
95th percentile	6.0×10^3	5.0	3.9×10^3	5.8	2.3×10^3	6.0

Author contributions.

Nahid Atashi: Writing original draft, Visualization, Methodology, Investigation, Formal analysis, Conceptualization. Xiaoyu Li: Writing – review and editing, Methodology, Data curation. Sasu Karttunen: Writing – review and editing, Methodology, Data curation, Technical support. Roy Harrison: Writing – review and editing, Methodology, Data curation. Matti Leinonen: Review and editing, Data providing. Jani Strömberg: Review and editing, Methodology, Data providing. Aino Kaltianen: Review and editing, Data curation. Riku Viri: Review and editing, Data providing. Laura Ruotsalainen: Writing – review

https://doi.org/10.5194/egusphere-2026-341
Preprint. Discussion started: 17 March 2026

and editing, Funding acquisition, Project administration. Leena Järvi: Writing – review and editing, Project administration, Investigation, Funding acquisition, Conceptualization.

Competing interests.

The authors declare that they have no conflict of interest.

Acknowledgements. The project was supported by the Research Council of Finland, CousCous (decision nr: 332177 and 332178) and AIforLesAuto (decision nr: 347197 and 347198), the RI-URBANS research and innovation program of the European Union Horizon 2020 (nr: 101036245), and Jane and Aatos Erkko Foundation for the RESTART project. The City of Helsinki is acknowledged for providing the plan for the new neighborhood. The PALM model system simulations were enabled by the Center for Scientific Computing (CSC) in Finland.

https://doi.org/10.5194/egusphere-2026-341
Preprint. Discussion started: 17 March 2026

References

Abd Razak, A., Hagishima, A., Ikegaya, N., and Tanimoto, J.: Analysis of airflow over building arrays for assessment of urban wind environment, Building and Environment, 59, 56–65, 2013.

Abhijith, K., Kumar, P., Gallagher, J., McNabola, A., Baldauf, R., Pilla, F., Broderick, B., Sabatino, S. D., and Pulvirenti, B.: Air pollution abatement performances of green infrastructure in open road and built-up street canyon environments – A review, Atmospheric Environment, 162, 71–86, https://doi.org/10.1016/j.atmosenv.2017.05.014, 2017.

Akinlabi, E., Maronga, B., Giometto, M. G., and Li, D.: Dispersive fluxes within and over a real urban canopy: a large-eddy simulation study, Boundary-Layer Meteorology, 185, 93–128, 2022.

Auvinen, M. and Karttunen, S.: P4UL Pre- and Post-Processing Python Library for Urban LES Simulations, GitHub, https://github.com/mjsauvinen/P4UL, last accessed: 18 April 2024, 2020.

Auvinen, M., Boi, S., Hellsten, A., Tanhuanpää, T., and Järvi, L.: Study of realistic urban boundary layer turbulence with high-resolution large-eddy simulation, Atmosphere, 11, 201, 2020.

Beddows, D. C. and Harrison, R. M.: PM10 and PM2. 5 emission factors for non-exhaust particles from road vehicles: Dependence upon vehicle mass and implications for battery electric vehicles, Atmospheric Environment, 244, 117 886, 2021.

Chen, L., Hang, J., Sandberg, M., Claesson, L., Di Sabatino, S., and Wigo, H.: The impacts of building height variations and building packing densities on flow adjustment and city breathability in idealized urban models, Building and Environment, 118, 344–361, 2017.

Cheng, W.-C., Liu, C.-H., Ho, Y.-K., Mo, Z., Wu, Z., Li, W., Chan, L. Y., Kwan, W., and Yau, H. T.: Turbulent flows over real heterogeneous urban surfaces: Wind tunnel experiments and Reynolds-averaged Navier-Stokes simulations, in: Building Simulation, vol. 14, pp. 1345–1358, Springer, 2021.

city of Helsinki: The Carbon-Neutral Helsinki 2035 Action Plan, 2018.

Du, Y., Isaxon, C., Roldin, P., Mattisson, K., Karttunen, S., Li, X., Malmqvist, E., and Järvi, L.: Large-eddy simulation of aerosol concentrations in a realistic urban environment: Model validation and transport mechanism, Environmental Pollution, 358, 124 475, 2024a.

Du, Y., Isaxon, C., Roldin, P., Mattisson, K., Karttunen, S., Li, X., Malmqvist, E., and Järvi, L.: Large-eddy simulation of aerosol concentrations in a realistic urban environment: Model validation and transport mechanism, Environmental Pollution, 358, 124 475, 2024b.

EEA: Trends and projections in Europe 2023, https://www.eea.europa.eu/publications/trends-and-projections-in-europe-2023, accessed: April 4, 2024, 2023.

Fenger, J.: Air pollution in the last 50 years–From local to global, Atmospheric Environment, 43, 13–22, 2009.

Fussell, J. C., Franklin, M., Green, D. C., Gustafsson, M., Harrison, R. M., Hicks, W., Kelly, F. J., Kishta, F., Miller, M. R., Mudway, I. S., et al.: A review of road traffic-derived non-exhaust particles: emissions, physicochemical characteristics, health risks, and mitigation measures, Environmental science & technology, 56, 6813–6835, 2022.

García-Sánchez, C., van Beeck, J., and Gorlé, C.: Predictive large eddy simulations for urban flows: Challenges and opportunities, Building and Environment, 139, 146–156, 2018.

Gousseau, P., Blocken, B., Stathopoulos, T., and Van Heijst, G.: CFD simulation of near-field pollutant dispersion on a high-resolution grid: a case study by LES and RANS for a building group in downtown Montreal, Atmospheric Environment, 45, 428–438, 2011.

Gromke, C. and Ruck, B.: Pollutant concentrations in street canyons of different aspect ratio with avenues of trees for various wind directions, Boundary-Layer Meteorology, 144, 41–64, 2012.

https://doi.org/10.5194/egusphere-2026-341
Preprint. Discussion started: 17 March 2026

Gronemeier, T. and Sühring, M.: On the effects of lateral openings on courtyard ventilation and pollution—a large-eddy simulation study, Atmosphere, 10, 63, 2019.

Gronemeier, T., Surm, K., Harms, F., Leitl, B., Maronga, B., and Raasch, S.: Validation of the dynamic core of the PALM model system 6.0 in urban environments: LES and wind-tunnel experiments, Geosci Model Develop Discuss, pp. 1–26, 2020.

Harms, F., Leitl, B., Schatzmann, M., and Patnaik, G.: Validating LES-based flow and dispersion models, Journal of Wind Engineering and Industrial Aerodynamics, 99, 289–295, 2011.

Harrison, R. M., Allan, J., Carruthers, D., Heal, M. R., Lewis, A. C., Marner, B., Murrells, T., and Williams, A.: Non-exhaust vehicle emissions of particulate matter and VOC from road traffic: A review, Atmospheric Environment, 262, 118 592, 2021.

Hassan, S., Akter, U. H., Nag, P., Molla, M. M., Khan, A., and Hasan, M. F.: Large-eddy simulation of airflow and pollutant dispersion in a model street canyon intersection of Dhaka city, Atmosphere, 13, 1028, 2022.

Helin, A., Niemi, J. V., Virkkula, A., Pirjola, L., Teinilä, K., Backman, J., Aurela, M., Saarikoski, S., Rönkkö, T., Asmi, E., et al.: Characteristics and source apportionment of black carbon in the Helsinki metropolitan area, Finland, Atmospheric Environment, 190, 87–98, 2018.

Hellsten, A., Ketelsen, K., Sühring, M., Auvinen, M., Maronga, B., Knigge, C., Barmpas, F., Tsegas, G., Moussiopoulos, N., and Raasch, S.: A nested multi-scale system implemented in the large-eddy simulation model PALM model system 6.0, Geoscientific Model Development, 14, 3185–3214, 2021.

Hertwig, D., Gough, H. L., Grimmond, S., Barlow, J. F., Kent, C. W., Lin, W. E., Robins, A. G., and Hayden, P.: Wake characteristics of tall buildings in a realistic urban canopy, Boundary-Layer Meteorology, 172, 239–270, 2019.

Hietikko, R., Kuuluvainen, H., Harrison, R. M., Portin, H., Timonen, H., Niemi, J. V., and Rönkkö, T.: Diurnal variation of nanocluster aerosol concentrations and emission factors in a street canyon, Atmospheric Environment, 189, 98–106, https://doi.org/10.1016/j.atmosenv.2018.06.031, 2018.

Hooftman, N., Messagie, M., Joint, F., Segard, J.-B., and Coosemans, T.: In-life range modularity for electric vehicles: The environmental impact of a range-extender trailer system, Applied Sciences, 8, 1016, 2018.

Hunt, J., Abell, C., Peters, A., and Woo, H.: Kinematical studies of the flows around free or surface-mounted obstacles; applying topology to flow visualization, Journal of Fluid Mechanics, 86, 179–200, 1978.

Järvi, L., Kurppa, M., Kuuluvainen, H., Rönkkö, T., Karttunen, S., Balling, A., Timonen, H., Niemi, J. V., and Pirjola, L.: Determinants of spatial variability of air pollutant concentrations in a street canyon network measured using a mobile laboratory and a drone, Science of The Total Environment, 856, 158 974, 2023.

Kiesewetter, G., Borken-Kleefeld, J., Schöpp, W., Heyes, C., Thunis, P., Bessagnet, B., Terrenoire, E., Gsella, A., and Amann, M.: Modelling NO 2 concentrations at the street level in the GAINS integrated assessment model: projections under current legislation, Atmospheric Chemistry and Physics, 14, 813–829, 2014.

Kokkola, H., Korhonen, H., Lehtinen, K., Makkonen, R., Asmi, A., Järvenoja, S., Anttila, T., Partanen, A.-I., Kulmala, M., Järvinen, H., et al.: SALSA–a sectional aerosol module for large scale applications, Atmospheric Chemistry and Physics, 8, 2469–2483, 2008.

Kurppa, M. and Strömberg, J.: Input files and scripts for creating PALM simulation input files on Mäkelänkatu in Helsinki, Finland (v1.1.0), Zenodo, https://doi.org/10.5281/zenodo.3839684, last access: 18 April 2024, 2020.

Kurppa, M., Hellsten, A., Auvinen, M., Raasch, S., Vesala, T., and Järvi, L.: Ventilation and air Quality in city blocks using large-eddy simulation—urban planning perspective, Atmosphere, 9, 65, 2018a.

https://doi.org/10.5194/egusphere-2026-341
Preprint. Discussion started: 17 March 2026

Kurppa, M., Hellsten, A., Roldin, P., Kokkola, H., Tonttila, J., Auvinen, M., Kent, C., Kumar, P., Maronga, B., and Järvi, L.: Implementation of the sectional aerosol module SALSA into the PALM model system 6.0: Model development and first evaluation, Geoscientific Model Development, 2018b.

Kurppa, M., Hellsten, A., Roldin, P., Kokkola, H., Tonttila, J., Auvinen, M., Kent, C., Kumar, P., Maronga, B., and Järvi, L.: Implementation of the sectional aerosol module SALSA2. 0 into the PALM model system 6.0: model development and first evaluation, Geoscientific Model Development, 12, 1403–1422, 2019.

Lehtomäki, H., Korhonen, A., Asikainen, A., Karvosenoja, N., Kupiainen, K., Paunu, V.-V., Savolahti, M., Sofiev, M., Palamarchuk, Y., Karppinen, A., et al.: Health impacts of ambient air pollution in Finland, International journal of environmental research and public health, 15, 736, 2018.

Leinonen, M., Al-Tachmeesschi, A., Turkmen, B., Atashi, N., and Ruotsalainen, L.: Long Short Term Memory Based Traffic Prediction Using Multi-Source Data, International Journal of Intelligent Transportation Systems Research, under review, 2024.

Lelieveld, J., Klingmüller, K., Pozzer, A., Pöschl, U., Fnais, M., Daiber, A., and Münzel, T.: Cardiovascular disease burden from ambient air pollution in Europe reassessed using novel hazard ratio functions, European heart journal, 40, 1590–1596, 2019.

Letzel, M. O., Krane, M., and Raasch, S.: High resolution urban large-eddy simulation studies from street canyon to neighbourhood scale, Atmospheric Environment, 42, 8770–8784, 2008.

Liu, Y., Chen, H., Gao, J., Li, Y., Dave, K., Chen, J., Federici, M., and Perricone, G.: Comparative analysis of non-exhaust airborne particles from electric and internal combustion engine vehicles, Journal of Hazardous Materials, 420, 126 626, 2021.

Liu, Y., Chen, H., Li, Y., Gao, J., Dave, K., Chen, J., Li, T., and Tu, R.: Exhaust and non-exhaust emissions from conventional and electric vehicles: A comparison of monetary impact values, Journal of Cleaner Production, 331, 129 965, 2022.

Makar, P. A., Stroud, C., Akingunola, A., Zhang, J., Ren, S., Cheung, P., and Zheng, Q.: Vehicle induced turbulence and atmospheric pollution, Atmospheric Chemistry and Physics Discussions, 2021, 1–38, 2021.

Maronga, B., Banzhaf, S., Burmeister, C., Esch, T., Forkel, R., Fröhlich, D., Fuka, V., Gehrke, K. F., Geletič, J., Giersch, S., et al.: Overview of the PALM model system 6.0, Geoscientific Model Development, 13, 1335–1372, 2020.

Mishra, A., Carpentieri, M., Robins, A., and Placidi, M.: Experimental study of the turbulent characteristics in the wake of tall building clusters, Flow, 4, E15, 2024.

Müller, M., Homleid, M., Ivarsson, K.-I., Køltzow, M. A., Lindskog, M., Midtbø, K. H., Andrae, U., Aspelien, T., Berggren, L., Bjørge, D., et al.: AROME-MetCoOp: A Nordic convective-scale operational weather prediction model, Weather and Forecasting, 32, 609–627, 2017.

National Land Survey of Finland: 2-meter elevation model for Finland, https://www.maanmittauslaitos.fi/en/maps-and-spatial-data/datasets-and-interfaces/product-descriptions/elevation-model-2-m, accessed: April 18, 2024, 2024.

Norwegian Meteorological Institute: File Interpolation, Manipulation and EXtraction library, Available at: https://wiki.met.no/fimex/start, last access: 18 April 2024.

Norwegian Meteorological Institute: MET Norway Thredds Service, Available online, https://thredds.met.no/thredds/catalog.html, last accessed: 18 April 2024, 2021.

Notter, B., Cox, B., Hausberger, S., Matzer, C., Weller, K., Dippold, M., Politschnig, N., Lipp, S., Allekotte, M., Knörr, W., André, M., Gagnepain, L., Hult, C., and Jerksjö, M.: HBEFA 4.2 Documentation of Updates, last access: 18 April 2024, 2022.

Park, S.-B., Baik, J.-J., Raasch, S., and Letzel, M. O.: A large-eddy simulation study of thermal effects on turbulent flow and dispersion in and above a street canyon, Journal of Applied Meteorology and Climatology, 51, 829–841, 2012.

https://doi.org/10.5194/egusphere-2026-341
Preprint. Discussion started: 17 March 2026

Pirjola, L., Kuuluvainen, H., Timonen, H., Saarikoski, S., Teinilä, K., Salo, L., Datta, A., Simonen, P., Karjalainen, P., Kulmala, K., et al.: Potential of renewable fuel to reduce diesel exhaust particle emissions, Applied Energy, 254, 113 636, 2019.

Piscitello, A., Bianco, C., Casasso, A., and Sethi, R.: Non-exhaust traffic emissions: Sources, characterization, and mitigation measures, Science of the Total Environment, 766, 144 440, 2021.

Resler, J., Bauerová, P., Belda, M., Bureš, M., Eben, K., Fuka, V., Geletič, J., Jareš, R., Karel, J., Keder, J., et al.: Challenges of high-fidelity air quality modeling in urban environments–PALM sensitivity study during stable conditions, EGUsphere, 2024, 1–35, 2024.

Rexeis, M. and Hausberger, S.: Trend of vehicle emission levels until 2020–Prognosis based on current vehicle measurements and future emission legislation, Atmospheric Environment, 43, 4689–4698, 2009.

Rönkkö, T. and Timonen, H.: Overview of sources and characteristics of nanoparticles in urban traffic-influenced areas, Journal of Alzheimer's disease, 72, 15–28, 2019.

Salim, S. M., Cheah, S. C., and Chan, A.: Numerical simulation of dispersion in urban street canyons with avenue-like tree plantings: comparison between RANS and LES, Building and Environment, 46, 1735–1746, 2011.

Shen, J., Cui, P., Huang, Y., Wu, Y., Luo, Y., Sin, C. H., and Guan, J.: New insights on precise regulation of pollutant distribution inside a street canyon by different vegetation planting patterns, Environmental Science and Pollution Research, 30, 63 148–63 174, 2023.

SoGA: SOGA, https://www.stateofglobalair.org/resources/report/state-global-air-report-2024, accessed: July 28, 2024, 2024.

Strömberg, J., Karttunen, S., and Auvinen, M.: Raster4H 2.0 (v2.1), https://doi.org/10.5281/zenodo.7442799, accessed: April 18, 2024, 2022.

Teinilä, K., Aurela, M., Niemi, J. V., Kousa, A., Petäjä, T., Järvi, L., Hillamo, R., Kangas, L., Saarikoski, S., and Timonen, H.: Concentration variation of gaseous and particulate pollutants in the Helsinki city centre–observations from a two-year campaign from 2013–2015, Boreal Environ. Res, 24, 115–136, 2019.

Teinilä, K., Saarikoski, S., Lintusaari, H., Lepistö, T., Marjanen, P., Aurela, M., Hellén, H., Tykkä, T., Lampimäki, M., Lampilahti, J., et al.: Measurement report: Wintertime aerosol characterization at an urban traffic site in Helsinki Finland, EGUsphere, 2024, 1–31, 2024.

Timmers, V. R. and Achten, P. A.: Non-exhaust PM emissions from electric vehicles, Atmospheric environment, 134, 10–17, 2016.

Tolias, I., Koutsourakis, N., Hertwig, D., Efthimiou, G., Venetsanos, A., and Bartzis, J.: Large Eddy Simulation study on the structure of turbulent flow in a complex city, Journal of Wind Engineering and Industrial Aerodynamics, 177, 101–116, 2018.

Tominaga, Y. and Stathopoulos, T.: Ten questions concerning modeling of near-field pollutant dispersion in the built environment, Building and Environment, 105, 390–402, 2016.

Torres, P., Le Clainche, S., and Vinuesa, R.: On the experimental, numerical and data-driven methods to study urban flows, Energies, 14, 1310, 2021.

Uehara, K., Murakami, S., Oikawa, S., and Wakamatsu, S.: Wind tunnel experiments on how thermal stratification affects flow in and above urban street canyons, Atmospheric Environment, 34, 1553–1562, 2000.

Vardoulakis, S., Fisher, B. E., Pericleous, K., and Gonzalez-Flesca, N.: Modelling air quality in street canyons: a review, Atmospheric environment, 37, 155–182, 2003.

Viri, R., Mäkinen, J., and Liimatainen, H.: Modelling car fleet renewal in Finland: A model and development speed-based scenarios, Transport Policy, 112, 63–79, 2021.

Vivienne, H.: Revision of EU air quality legislation: Setting a zero pollution objective for air, accessed: July 29, 2024, 2023.

VTT: GEVO 2020 - Helsinki, https://iea.blob.core.windows.net/assets/db408b53-276c-47d6-8b05-52e53b1208e1/e-bus-case-study-Helsinki.pdf, accessed: April 16, 2024, 2018.

https://doi.org/10.5194/egusphere-2026-341
Preprint. Discussion started: 17 March 2026

Xie, X., Huang, Z., and Wang, J.-s.: Impact of building configuration on air quality in street canyon, Atmospheric Environment, 39, 4519–4530, 2005.

Yassin, M. F. and Ohba, M.: Experimental simulation of air quality in street canyon under changes of building orientation and aspect ratio, Journal of Exposure Science & Environmental Epidemiology, 22, 502–515, 2012.

Yazid, A. W. M., Sidik, N. A. C., Salim, S. M., and Saqr, K. M.: A review on the flow structure and pollutant dispersion in urban street canyons for urban planning strategies, Simulation, 90, 892–916, 2014.

Zhang, Y., Ou, C., Chen, L., Wu, L., Liu, J., Wang, X., Lin, H., Gao, P., and Hang, J.: Numerical studies of passive and reactive pollutant dispersion in high-density urban models with various building densities and height variations, Building and Environment, 177, 106 916, 2020.

Zhang, Y., Ye, X., Wang, S., He, X., Dong, L., Zhang, N., Wang, H., Wang, Z., Ma, Y., Wang, L., et al.: Large-eddy simulation of traffic-related air pollution at a very high resolution in a mega-city: evaluation against mobile sensors and insights for influencing factors, Atmospheric Chemistry and Physics, 21, 2917–2929, 2021.

Zheng, X., Montazeri, H., and Blocken, B.: Impact of building façade geometrical details on pollutant dispersion in street canyons, Building and Environment, 212, 108 746, 2022.